Chinese Journal of Aeronautics, (2014),27(2): 438–444

Chinese Society of Aeronautics and Astronautics
& Beihang University

Chinese Journal of Aeronautics

cja@buaa.edu.cn
www.sciencedirect.com

Microstructure evolution of a hypereutectic Nb–Ti–Si–Cr–Al–Hf alloy processed by directional solidification

Ding Fei, Jia Lina, Yuan Sainan, Su Linfen, Weng Junfei, Zhang Hu *

School of Materials Science and Engineering, Beihang University, Beijing 100191, China

Received 6 March 2013; revised 9 May 2013; accepted 24 June 2013
Available online 2 August 2013

KEYWORDS

Directional solidification;
Fiber-mesh structure;
Heat treatment;
Microstructure evolution;
Nb_{ss} + Nb_5Si_3 eutectics;
Solute diffusion;
Volume fraction

Abstract In this work, the Nb–14Si–24Ti–10Cr–2Al–2Hf–0.1Y alloy (at.%) was processed by the liquid–metal-cooled directional solidification (DS) at 1750 °C with withdrawal rates of 1.2, 6, 18 mm/min and post heat treatment (HT) at 1450 °C for 10 h. The microstructures of the directionally solidified and heat treated samples were investigated. The results show that the microstructure of directionally solidified alloy mainly consists of petaloid Nb_{ss} + Nb_5Si_3 eutectics and Ti-rich Nb_{ss} + Nb_5Si_3 + Cr_2Nb eutectics. With the increase of withdrawal rate, the primary Nb_5Si_3 is eliminated, Nb_{ss} + Nb_5Si_3 eutectic cells turn round and connected with the microstructure refinement and Nb_{ss} + Nb_5Si_3 + Cr_2Nb eutectics turn to a river-like morphology. After heat treatment, Nb_{ss} + Nb_5Si_3 + Cr_2Nb eutectics disappeared and petaloid Nb_{ss} + Nb_5Si_3 eutectics turn to a specific fiber-mesh structure gradually, which is promoted by higher withdrawal rates. Furthermore, both the volume fraction of Cr_2Nb and the content of Cr in Nb_{ss} of Nb_{ss} + Nb_5Si_3 eutectics change regularly with the increase of withdrawal rate and heat treatment at 1450 °C for 10 h.

1. Introduction

Niobium–silicides based alloys are expected to be promising candidate materials for the next generation of aircraft engine due to their notably high melting points, moderate density, high stiffness and good strength retention at high temperatures.[1–5] In niobium–silicides based alloys, Nb solid solution (Nb_{ss}) provides the ambient temperature fracture toughness, the silicides (Nb_5Si_3 and Nb_3Si) supply high temperature strength and Cr_2Nb with silicides together contributes to high temperature oxidation resistance.[6,7] Characteristics of the above constituent phases including the fraction volume, morphology, distribution and composition have an impact on the balance of properties at both ambient and high temperatures.[8–10] Therefore, microstructure controlling and optimizing of Nb–Si based alloys are of great significance.

In previous work,[11] we investigated the microstructures and properties of Nb–16Si–22Ti–2Al–2Hf–17Cr alloy. However, the large-size silicides in the hypereutectic alloys prejudiced the room temperature fracture toughness. In order to obtain excellent fracture toughness, Si addition was decreased to

* Corresponding author. Tel.: +86 10 82316958.
E-mail address: zhanghu@buaa.edu.cn (H. Zhang).

Peer review under responsibility of Editorial Committee of CJA.

Production and hosting by Elsevier

http://dx.doi.org/10.1016/j.cja.2013.07.032

eliminate primary silicides and minor active element Y[12] was added to reduce the content of the impurity elements.

In addition to the alloy composition, processing technologies are effective means to optimize the microstructure,[13,14] and directional solidification has been proved to improve the high temperature strength with Nb_{ss} and intermetallic phases well aligned along the growth direction.[15,16] Moreover, appropriate heat treatment could alleviate solute segregation and eliminate unstable phases.[17,18]

In this study, an Nb–14Si–24Ti–10Cr–2Al–2Hf–0.1Y (at.%) alloy was directionally solidified by liquid–metal-cooled method and then heat treated. The purpose of this the present work was to investigate the effects of withdrawal rate and heat treatment on the morphology, distribution, composition and volume fraction of the constituent phases.

2. Experimental

With the nominal composition of Nb–14Si–24Ti–10Cr–2Al–2Hf–0.1Y, a master alloy button, weighing approximately 1.5 kg, was prepared by vacuum non-consumable arc-melting (VCAM). The alloy button was melted four times to ensure chemical homogeneity. Master alloy rods with 13 mm in diameter were cut from the ingot by electro-discharge machining (EDM). An Al_2O_3 crucible with layer of high purity Y_2O_3 in the interior wall surface was used for directional solidification. Directional solidification was conducted in a vertical Bridgman furnace and liquid metal cooling method. After holding for 20 min at 1750 °C in the atmosphere of argon, samples were withdrawn at 1.2, 6, 18 mm/min respectively and the withdrawal distance was set to be 160 mm. The samples were cut open longitudinally from the middle, half of which were then heat treated at 1450 °C for 10 h in a high vacuum heat treatment furnace. Directionally solidified samples at 1.2, 6, 18 mm/min were marked as DS1.2, DS06, DS18, and the subsequent heat treated samples were marked as HT1.2, HT06, HT18. All the samples were chosen from the steady-state area. Microstructure analysis was performed in a scanning electron microscope (SEM, QUANTA600) equipped with an energy dispersive X-ray spectroscopy (EDS, INCAPentaFETx3). The EDS results given in this paper were average values of three measurements. The phases were identified by the X-ray diffraction (XRD, D/max2200pc, Cu K_α).

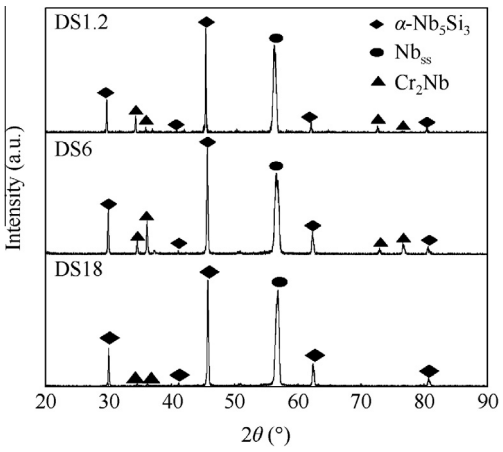

Fig. 1 XRD patterns of DS samples with different withdrawal rates.

3. Results and discussion

3.1. Microstructure of directionally solidified (DS) samples

Fig. 1 illustrates the XRD patterns of DS samples with different withdrawal rates. Combining EDS results shown in Table 1, it can be confirmed that the DS samples are composed of Nb_{ss}, Nb_5Si_3 and Cr_2Nb. As shown in Fig. 1, the type of constituent silicide was α-Nb_5Si_3, forming in the $D8_1$ body-centered tetragonal structure. The structure type of Nb_5Si_3 did not change with the withdrawal rate increasing from 1.2 mm/min to 18 mm/min.

Fig. 2 presents the typical backscattered electron (BSE) micrographs of the directionally solidified alloy with different withdrawal rates at a constant temperature of 1750 °C. Microstructures of DS samples mainly consisted of Nb_{ss} + Nb_5Si_3 eutectics and Ti-rich Nb_{ss} + Nb_5Si_3 + Cr_2Nb eutectics located between the Nb_{ss} + Nb_5Si_3 eutectic cells. From the transverse sections of DS specimens in Fig. 2(e)–(h), it could be seen that Nb_{ss} + Nb_5Si_3 eutectic cells, in which the granular or rod-like Nb_{ss} were distributed in the Nb_5Si_3 matrix, were tetragonal or nearly round. Fine granular Nb_{ss} tended to gather in the center of eutectic cells, while in the exterior margin, rod-like Nb_{ss} were largely perpendicular to boundaries of the eutectic cells. Nb_{ss} and Nb_5Si_3 grew radially from the interior to the boundaries of eutectic cells in a coupled manner, and hence Nb_{ss} + Nb_5Si_3 eutectic cells

Table 1 Compositions of constituent phases in DS samples determined by EDS (at.%).

Sample	Phase	Nb	Si	Ti	Al	Cr	Hf
DS1.2	$Nb_5Si_3^*$	31.55	28.36	30.11	1.36	5.07	3.55
	Nb_{ss}	69.43	3.05	18.41	1.84	6.47	0.80
	Nb_5Si_3	45.44	36.13	15.18	0.60	0.37	2.28
	Cr_2Nb	24.21	10.90	14.23	0.71	47.39	2.55
DS06	Nb_{ss}	61.34	4.09	22.07	2.09	9.37	1.04
	Nb_5Si_3	44.52	36.02	15.70	0.91	0.50	2.44
	Cr_2Nb	22.29	10.78	15.59	0.84	47.31	3.19
DS18	Nb_{ss}	60.38	3.52	22.38	2.09	10.59	1.04
	Nb_5Si_3	46.93	35.85	14.15	0.64	0.44	1.99
	River-like eutectic Nb_{ss} + Nb_5Si_3 + Cr_2Nb	28.13	12.19	28.94	1.85	25.64	3.25

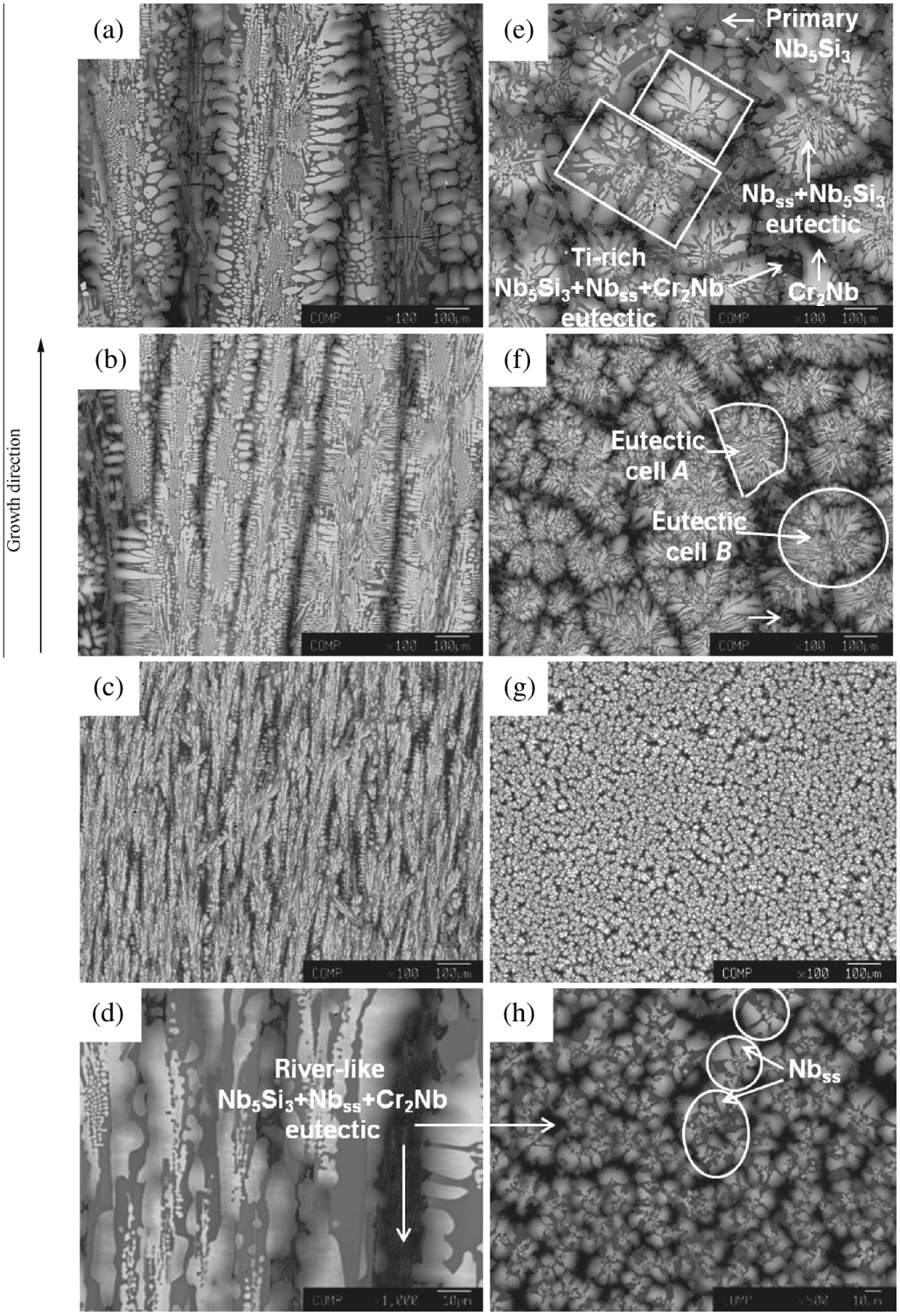

Fig. 2 Typical microstructures of directionally solidified Nb–14Si–24Ti-10Cr–2Al–2Hf–0.1Y alloy on both longitudinal ((a)–(d)) and transverse ((e)–(h)) sections with withdrawal rates of ((a), (e)) 1.2 mm/min; ((b), (f)) 6 mm/min; ((c), (g), (d), (h)) 18 mm/min.

presented a petaloid morphology, as shown in Fig. 2(e) and (f). From the longitudinal sections of the DS specimens in Fig. 2(a–(d), it could be seen that both Nb_{ss} + Nb_5Si_3 eutectics and Nb_{ss} + Nb_5Si_3 + Cr_2Nb eutectics were aligned erectly along the growth direction and the interfaces of Nb_{ss} + Nb_5Si_3 eutectics were distinct.

The withdrawal rate affected significantly on microstructures of directionally solidified specimens. In DS1.2 sample, there existed primary Nb_5Si_3 blocks (marked as $Nb_5Si_3^*$) as well. The average width of the blocks was about 35 μm.The sharp and straight edges of $Nb_5Si_3^*$ indicated a typical feature of facet growth, as shown in Fig. 2(e). However, with the

increase of withdraw rate, $Nb_5Si_3^*$ disappeared in DS06 and DS18 samples. This change closely related to the deviation of Nb + Nb_5Si_3 pseudo-eutectic area during non-equilibrium solidification. For an alloy with eutectic reaction, it was believed that[19,20] when the melting points of constituent phases were different, pseudo-eutectic area would locate to the side of one with higher melting point and higher solidification rate would cause greater deviation. Hence, for Nb-Si alloy, eutectic point of Nb + Nb_5Si_3 would deviate gradually to the side of Nb_5Si_3 with the increase of withdrawal rate. For the hypereutectic composition investigated, hypereutectic microstructure would gradually convert into eutectics with the increase of withdrawal rate.

The average diameter of Nb_{ss} + Nb_5Si_3 eutectic cells in DS1.2 was 330.7 ± 23.5 μm, while in DS06 and DS18 samples, it changed to 235.8 ± 12.7 μm and 25.0 ± 1.2 μm respectively. While the size of Nb_{ss} + Nb_5Si_3 eutectics decreased with the increase of withdrawal rate, their volume fraction increased. Furthermore, the morphology of Nb_{ss} + Nb_5Si_3 eutectic cells changed obviously. From transverse sections it could be seen that the boundaries of Nb_{ss} + Nb_5Si_3 eutectic cells in DS1.2 were mainly tetragonal (as shown by the two rectangles in Fig. 2(e)), while in DS06 and DS18 they turned smoother and rounder. As shown in Fig. 2(f), the boundary of cell A and cell B in DS06 sample were semicircular and round respectively. In DS18 sample, with the microstructure refinement, Nb_{ss} + Nb_5Si_3 eutectic cells turned smoother and Nb_{ss} in the exterior margin of eutectic cells became connected, as shown in Fig. 2(h).

With the increase of withdrawal rate, both the volume fraction of Nb_{ss} + Nb_5Si_3 + Cr_2Nb eutectics decreased and Cr_2Nb decreased. The volume fraction of Cr_2Nb decreased from 5.8% in DS1.2 to 3.1% in DS06 approximately. While in DS18 sample, the volume fraction of Cr_2Nb was less than 1%. This change affected the morphology of Cr_2Nb in Nb_{ss} + Nb_5Si_3 + Cr_2Nb eutectics. In DS1.2, with a high content in Nb_{ss} + Nb_5Si_3 + Cr_2Nb eutectics, most Cr_2Nb acted as the matrix in which small amounts of Ti-rich Nb_{ss} and Nb_5Si_3 were located. There even existed single-phase Cr_2Nb outside the region of Nb_{ss} + Nb_5Si_3 + Cr_2Nb eutectics as shown in Fig. 2(e). With the increase of withdrawal rate, the single-phase Cr_2Nb disappeared. In DS18 sample, with a decreased content of Cr_2Nb in Nb_{ss} + Nb_5Si_3 + Cr_2Nb eutectics, the constituent phases in Nb_{ss} + Nb_5Si_3 + Cr_2Nb eutectics distributed evenly and uniformly, presenting a river-like eutectic morphology, as shown in Fig. 2(d) and (h).

3.2. Microstructure of the subsequent heat treatment (HT) samples

Fig. 3 illustrates the XRD patterns of HT samples with different withdrawal rates. Combining EDS results shown in Table 2, it can be seen that HT samples were also composed of Nb_{ss}, α-Nb_5Si_3 and Cr_2Nb. The structure type of Nb_5Si_3 did not change after heat treatment at 1450 °C for 10 h.

Fig. 4 illustrates the microstructures on both transverse and longitudinal sections of the HT samples. Microstructures of HT samples changed notably compared with DS samples. Fine Nb_{ss} slices in the center of Nb_{ss} + Nb_5Si_3 eutectics connected together, and even connected with the coarser Nb_{ss} in the exterior margin of Nb_{ss} + Nb_5Si_3 eutectics. Thus, Nb_{ss} turned

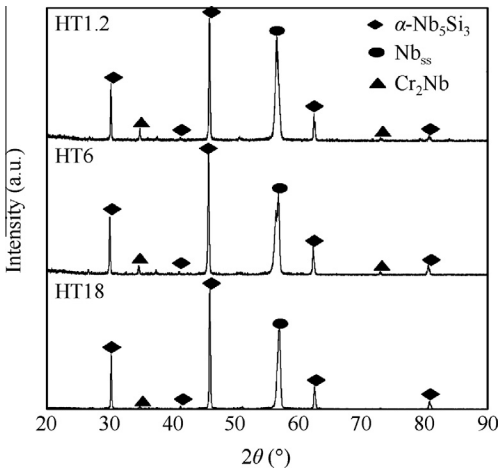

Fig. 3 XRD patterns of HT samples with different withdrawal rates.

Table 2 Compositions of constituent phases in DS samples determined by EDS (at.%).

Sample	Phases	Nb	Si	Ti	Al	Cr	Hf
HT1.2	$Nb_5Si_3^*$	28.15	36.79	26.23	1.21	1.57	6.05
	Nb_{ss}	63.92	2.09	20.59	1.63	11.02	0.75
	Nb_5Si_3	46.62	35.89	14.41	0.70	0.35	2.03
	Cr_2Nb	22.89	10.60	15.03	0.78	47.70	3.00
HT06	Nb_{ss}	53.88	2.42	27.35	2.26	12.98	1.11
	Nb_5Si_3	41.57	36.58	17.59	0.61	0.54	3.11
	Cr_2Nb	23.71	9.51	13.89	0.83	49.55	2.51
HT18	Nb_{ss}	55.34	2.52	27.39	2.31	11.31	1.13
	Nb_5Si_3	47.32	35.80	13.82	0.72	0.34	2.00

continuous to form a meshy matrix. With smoother boundaries, Nb_5Si_3 were inclined to be spheroidized and distributed discretely as fibers in the meshy matrix of Nb_{ss}. Therefore, a specific fiber-mesh structure was obtained, as shown in Fig. 4(e), (f) and (g).

With the connection of Nbss, the boundaries of Nb_{ss} + Nb_5Si_3 eutectic cells turned blurry and the shape of transverse sections was no longer regularly round or tetragonal. Furthermore, Ti-rich Nb_{ss} + Nb_5Si_3 + Cr_2Nb eutectics disappeared while Cr_2Nb still remained, as shown in Fig. 4 (d) and (e). After heat treatment, the volume fraction of Cr_2Nb decreased from 3.0% in HT1.2 to 1.4% in HT06 approximately. While in HT18, the volume fraction of Cr_2Nb was less than 1%.

In HT samples, with the increase of withdrawal rate, the volume fraction of the fiber-mesh structure increased while the petaloid Nb_{ss} + Nb_5Si_3 eutectics decreased. In HT 1.2 sample, in the region beyond the petaloid Nb_{ss} + Nb_5Si_3 eutectics, Nb_5Si_3 stayed continuous as matrix though Nb_{ss} had connected to some extent, as shown in Fig. 4(d). Therefore, the fiber-mesh structure mentioned above was not formed yet. In HT06 sample, the newly-formed fiber-mesh structure was distinguished with petaloid Nb_{ss} + Nb_5Si_3 eutectic cells, as shown in Fig. 4(e). While in HT18, the microstructure had totally transformed from petaloid Nb_{ss} + Nb_5Si_3 eutectics to the specific fiber-mesh structure, as shown in Fig. 4(f) and

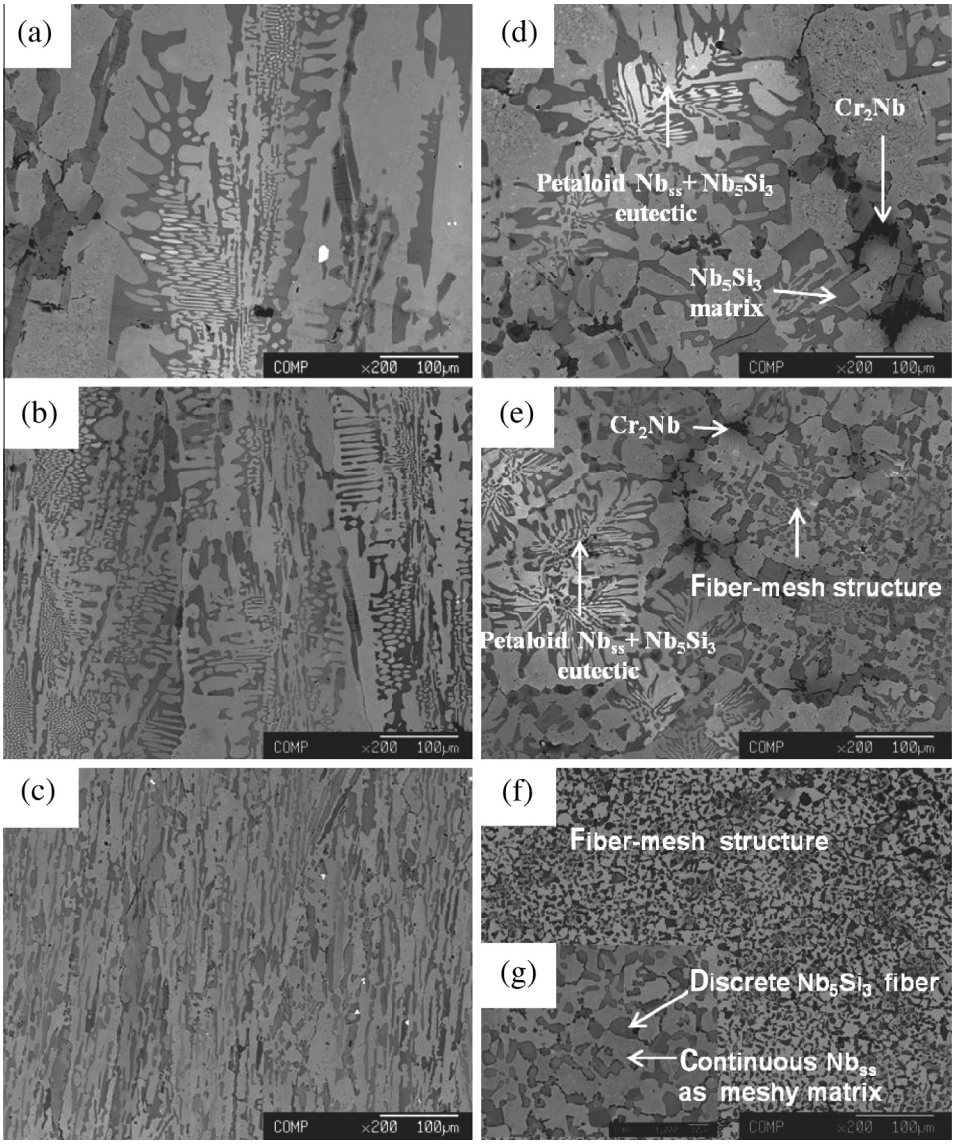

Fig. 4 Typical microstructures on longitudinal ((a)–(c)) and transverse sections ((d)–(g)) of the HT samples with DS withdrawal rates of ((a), (d)) 1.2 mm/min; ((b), (e)) 6 mm/min; ((c), (f), (g)) 18 mm/min.

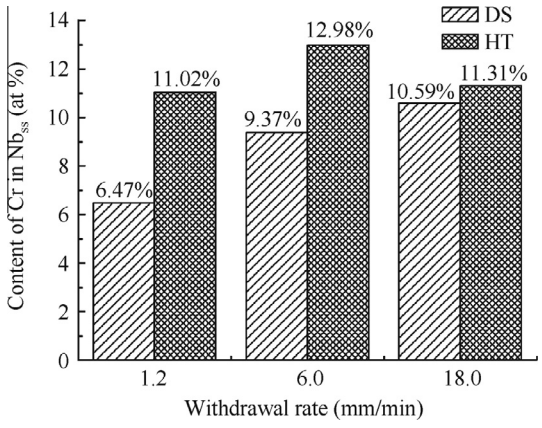

Fig. 5 Content change of Cr in Nb_{ss} with the increase of withdrawal rate in DS and HT samples.

(g). This finding revealed that higher withdrawal rate could promote the microstructure transformation above during this heat treatment.

4. Discussion

4.1. Solidification path

The EDS result of the river-like Nb_5Si_3 + Nb_{ss} + Cr_2Nb eutectic in Fig. 2h was shown in Table 1. It could be seen that the contents of Ti and Cr, whose freezing points were relatively low, were both higher than their contents in Nb_{ss} + Nb_5Si_3 + Cr_2Nb eutectic. Combining this result with the fact that the Nb_5Si_3 + Nb_{ss} + Cr_2Nb eutectics existed in the intercellular region, it could be accordingly deduced that Nb_5Si_3 + Nb_{ss} + Cr_2Nb eutectics were solidified after Nb_{ss} + Nb_5Si_3 eutectics during directional solidification. Therefore, the solidification path of the DS18 sample was

concluded as $L \rightarrow Nb_{ss} + Nb_5Si_3$ eutectic + L_1, $L_1 \rightarrow$ Ti-riched $Nb_5Si_3 + Nb_{ss} + Cr_2Nb$ eutectic. However, when withdraw rate was 1.2 mm/min, $Nb_5Si_3^*$ blocks precipitated earlier before $Nb_{ss} + Nb_5Si_3$ eutectic as primary silicide, and hence the solidification path was described as $L \rightarrow Nb_5Si_3^* + L_1$, $L_1 \rightarrow Nb_{ss} + Nb_5Si_3$ eutectic + L_2, $L_2 \rightarrow$ Ti-riched $Nb_5Si_3 + Nb_{ss} + Cr_2Nb$ eutectic. Due to the disappearance of $Nb_5Si_3^*$, the solidification path of DS06 was identical with DS18.

4.2. Content change of Cr

As shown in Table 1 and Table 2, Cr tended to be solid dissolved in Nb_{ss} instead of Nb_5Si_3. In DS samples, with the increase of withdrawal rate, the content of Cr in Nb_{ss} increased and the maximum reached 10.59 at.% in DS18. Meanwhile, the volume fraction of Cr_2Nb decreased. After heat treatment, the content of Cr in Nb_{ss} increased further with the continuous decrease of Cr_2Nb. Fig. 5 illustrates the content change of Cr in Nb_{ss} with the increase of withdrawal rate in DS and HT samples.

Three factors as follows were supposed to account for the increase of Cr in Nb_{ss} with the increase of withdrawal rate in DS samples. Firstly, high withdrawal rate accelerated the solidification of Nb_{ss}, which hindered the diffusion of low-melting point elements including Cr and Ti from Nb_{ss} to the residual liquid. Hence, the increase of Cr in Nb_{ss} was observed in DS samples. Secondly, primary silicide $Nb_5Si_3^*$ existed in DS1.2 sample and the content of Cr in $Nb_5Si_3^*$ reached 5.07at%. When $Nb_5Si_3^*$ disappeared at higher withdraw rates, Cr in $Nb_5Si_3^*$ would diffuse to adjacent phases including Nb_{ss}, Nb_5Si_3 and Cr_2Nb. According to Table 1, Cr in Nb_5Si_3 did not noticeably increase and the volume fraction of Cr_2Nb even decreased. Thus, Cr in $Nb_5Si_3^*$ was bound to diffuse into Nb_{ss}. Thirdly, the content of Cr in Nb_{ss} was closely related with the content of Ti in Nb_{ss}. Zelenitsas et al.[21] concluded through investigation that Cr content in Nb_{ss} grew up with the increase of Ti/Nb ratio in Nb_{ss}. It could be seen from Table 1 that, with the increase of withdrawal rate, the content of Ti in Nb_{ss} increased while the content of Nb went the other way, which pushed up the Ti/Nb ratio and hence caused the increase of Cr content in Nb_{ss}.

After heat treatment, the content of Cr in Nb_{ss} increased further. This change was thought to be related with the decrease of Cr_2Nb. Cr in Cr_2Nb would diffuse to adjacent phases including Nb_5Si_3 and Nb_{ss}. While Cr in Nb_5Si_3 did not increase noticeably, the majority of Cr diffused into Nb_{ss}. Furthermore, Ti/Nb ratio in Nb_{ss} increased further after heat treatment, which could also promote the solid solution content of Cr in Nb_{ss}.

As described in Section 3.1, the volume fraction of Cr_2Nb decreased with the increase of withdrawal rate in DS samples. This change closely related to solute diffusion during solidification. As analyzed in Section 4.1, $Nb_{ss} + Nb_5Si_3$ eutectics were preferential precipitated compared to Cr_2Nb in low-melting point region. High withdrawal rate accelerated the solidification of $Nb_{ss} + Nb_5Si_3$ eutectics, hindering the diffusion of low-melting point elements including Cr and Ti from $Nb_{ss} + Nb_5Si_3$ eutectic to the residual liquid, which could be confirmed with the increase of Cr and Ti in Nb_{ss} as shown in Table 1 and Table 2. Hence, the content of Cr in residual liquid decreased, which caused the volume fraction decrease of Cr_2Nb.

As a significant alloying element to Nb–Si based composites, the content of Cr in both compounded and dissociative forms would definitely affect the materials performance such as oxidation resistance at high temperature and fracture toughness at room temperature.[22,23] In this work, Cr content in Nb_{ss} and the volume fraction of Cr_2Nb could be both regularly controlled through the withdrawal rate of directional solidification and the subsequent heat treatment.

5. Conclusions

(1) The microstructure of directionally solidified Nb–14Si–24Ti–10Cr–2Al–2Hf–0.1Y alloy mainly consisted of $Nb_{ss} + Nb_5Si_3$ eutectics and Ti-rich $Nb_{ss} + Nb_5Si_3 + Cr_2Nb$ eutectics. As the withdrawal rate increased, the primary Nb_5Si_3 was eliminated, $Nb_{ss} + Nb_5Si_3$ eutectic cells turned round and connected and $Nb_{ss} + Nb_5Si_3 + Cr_2Nb$ eutectics turned to a river-like morphology gradually.

(2) After heat treatment, petaloid $Nb_{ss} + Nb_5Si_3$ eutectics transformed to a specific fiber-mesh structure, which was promoted by higher withdrawal rates. Ti-riched $Nb_{ss} + Nb_5Si_3 + Cr_2Nb$ eutectics disappeared while Cr_2Nb still remained.

(3) In DS samples, with the increase of withdrawal rate, the content of Cr in Nb_{ss} increased while the volume fraction of Cr_2Nb decreased. After heat treatment, the content of Cr in Nb_{ss} increased further with the continuous decrease of Cr_2Nb.

Acknowledgement

This study was supported by National Natural Science Foundation of China (No. 51101005).

References

1. Perepezko JH. The hotter the engine, the better. *Science* 2009;**326**:1068–9.
2. Bewlay BP, Jackson MR, Zhao JC, Subramanian PR. A review of very high-temperature Nb–Si based composites. *Metall Mater Trans A* 2003;**34**(10):2043–52.
3. Bewlay BP, Jackson MR. The balance of mechanical and environmental properties of a multielement niobium–niobium silicide-based in situ composite. *Metall Mater Mater Trans A* 1996;**27**(12):3801–8.
4. Bewlay BP, Jackson MR, Gigliotti M. Niobium silicide high temperature in-situ composites. *Intermetall Compd – Principles Pract: Prog* 2002;**3**:541–60.
5. Ma LM, Tang XX, Wang B, Jia LN, Yuan SN, Zhang H. Purification in the interaction between yttria mould and Nb–silicide-based alloy during directional solidification: a novel effect of yttrium. *Scripta Mater* 2012;**67**(3):233–6.
6. Su LF, Jia LN, Feng YB, Zhang HR, Yuan SN, Zhang H. Microstructure and room-temperature fracture toughness of directionally solidified Nb–Si–Ti–Cr–Al–Hf alloy. *Mater Sci Eng, A* 2013;**560**:672–7.
7. Yuan SN, Jia LN, Ma LM, Cui RJ, Su LF, Zhang H. The microstructure optimizing of the Nb–14Si–22Ti–4Cr–2Al–2Hf alloy processed by directional solidification. *Mater Lett* 2012;**84**(10):124–7.

8. Qu SY, Han YF, Song LG. Effects of alloying elements on phase stability in Nb–Si system intermetallics materials. *Intermetallics* 2007;**15**(5–6):810–3.
9. Kim WY, Tanaka H, Kasama A, Hananda S. Microstructure and room temperature fracture toughness of Nbss/Nb5Si3 in situ composites. *Intermetallics* 2001;**9**(9):827–34.
10. Sha JB, Hirai H, Tabaru T, Kitahara A, Hanada S. Mechanical properties of as-cast and directionally solidified Nb–Mo–W–Ti–Si in-situ composites at high temperatures. *Metall Mater Trans A* 2003;**34**(1):85–94.
11. Li XJ, Chen HF, Sha JB, Zhang H. The effects of melting technologies on the microstructures and properties of Nb-16Si-22Ti-2Al-2Hf-17Cr alloy. *Mater Sci Eng A* 2010;**527**(23):6140–52.
12. Qu SY, Han YF, Song JX, Xiao CB, Song LG. Effects of Y and Ce on microstructures and properties of Nb-Si system composites. *J Rare Earths* 2004;**22**(z1):197–200.
13. Jackson MR, Bewlay BP, Rowe RG, Skelly DW, Lipsitt HA. High-temperature refractory metal-intermetallic composites. *JOM* 1996;**48**(1):39–43.
14. Bewlay BP, Jackson MR, Zhao JC, Subramanian PR, Mendiratta JJ, Lewandowski JJ. Ultrahigh-temperature Nb-silicide-based composites. *MRS Bull* 2003;**28**(9):646–53.
15. Sekido N, Kimura Y. Fracture toughness and high temperature strength of unidirectionally solidified Nb–Si binary and Nb–Ti–Si ternary alloys. *J Alloy Compd* 2006;**425**(1–2):223–9.
16. Wang LG, Ding F, Yuan SN, Jia LN, Zhang H. The effects of the withdrawal rate and heat treatment on the microstructure of directionally solidified Nb–14Si–24Ti alloy. *High Temp Mater Proc* 2012;**32**(2):113–8.
17. Guo BH, Guo XP. Effect of high temperature treatments on microstructure of Nb–Ti–Cr–Si based ultrahigh temperature alloy. *Trans Nonferrous Metal Soc China* 2011;**21**:1710–6.
18. Guo HS, Guo XP. Effects of homogenizing and aging treatments on the microstructure and microhardness of an Nb–ilicide based ultrahigh temperature alloy. *Int J Mater Ref* 2010;**101**(7):900–5.
19. Hu GX, Cai X, Rong YH. *Fundamentals of material science*. Shanghai: Shanghai Jiaotong University Press; 2006.
20. Hu HQ, Shen NF, Yao S. *Metal solidification principle*. Beijing: China Machine Press; 2000.
21. Zelenitsas K, Tsakiropoulos P. Study of the role of Ta and Cr additions in the microstructure of Nb–Ti–Si–Al in situ composites. *Intermetallics* 2006;**14**(6):639–59.
22. Chan KS. Alloying effects on fracture mechanisms in Nb-based intermetallic in-situ composites. *Mater Sci Eng A* 2002;**329–331**:513–22.
23. Grammenos I, Tsakiropoulos P. Study of the role of Al, Cr and Ti additions in the microstructure of Nb–18Si–5Hf base alloys. *Intermetallics* 2010;**18**(2):242–53.

Ding Fei received his master degree at School of Materials Science and Engineering, Beihang University,Beijing,China in the year of 2014. He followded Supervisor Zhang to research on microsturcture control and optimization of high temperature structure materials.

Zhang Hu is a professor and Ph.D. supervisor at School of Materials Science and Engineering, Beihang University, Beijing, China. He received the Ph.D. degree from Harbin Institute of Technology (HIT) in 1990. His current research interests are solidification and control of metal materials, high temperature structure materials and automatic control during hot-working treatment.